On the influence of coupled and uncoupled fluid dynamic models in a large scale journal bearing.

J.M. Crous, P.S Heyns, J. Dirker

Department of Mechanical and Aeronautical Engineering, University of Pretoria, South Africa

Abstract

This study considers the extent to which the coupling of the governing equations influences the fluid dynamics of a large-scale turbo generator journal bearing. The study was conducted by formulating and implementing four fluid models in the OpenFOAM open-source CFD package. The fluid models are constructed so that uncoupled, weakly-coupled and strongly-coupled model formulations can be studied. To reduce the computational costs, a three-dimensional region of the oil film was extracted and considered. This small region was selected because the computational costs would have been extremely high for a full-scale simulation. To this end, the section selected for extraction was the region where the fluid dependencies are known to exert the greatest influence on the fluid behaviour. It was found that for both the weak-coupled and strong-coupled models, the coupling influenced the flow significantly. The extent to which the coupling influenced the fluid behaviour was seen to be dependent on the strength of the coupling, the dependency that introduced the coupling as well as the formulation of the fluid model. The weak-coupling introduced a greater qualitative change where the influence of the coupling was up to half the influence of the pressure dependence. The strong-coupling showed a greater change in the fluid behaviour and the flow departed non-uniformly from the uncoupled models.

Keywords

Strong-coupling; Weak-coupling; Viscosity dependencies; Viscoelastic fluid formulation; Non-isothermal; Journal bearings

1. Introduction

In most research pertaining to the dynamics of rotor-bearing systems, as found in steam turbines for power generation, has used only simplified fluid models. Owing to the various complexities that arise when modelling the rotor-bearing system. The dynamics of the journal bearing influence the dynamics of the entire system, since the bearing supports the rotor. At the same time, studies have been done on the influence of lubricant dependencies on the dynamics of the journal and have highlighted its importance [1], [2]. Since the bearing acts as a support for the rotor, it follows that factors influencing the dynamics of the bearing will influence the dynamics of the rotor [3].

In the classical formulation of the rotor-dynamics problem, the Reynolds equation is used to compute the pressure distribution inside the bearing. The restrictions of this classical model are well known: viscosity dependencies are neglected, the film thickness is assumed to be negligible and nonlinear fluid behaviour is neglected. Consequently the model has been extended to account for various kinds of dependencies [2].

The prominence of dependencies has been augmented in recent years due to the addition of various additives to the base oil. The rapid development of oil and bearing technologies and the increased

importance of the dependencies have rendered the classical formulation of the problem inapplicable [4].

Mang and Drensel [5] note that the three most prominent dependencies of the lubricant film, which influence the operating conditions of the bearing, are pressure, temperature and shear rate. The influence of the viscoelastic behaviour of the fluid film, due to the addition of polymer additives have been highlighted by Gwynllyw et al. [2]. Moreover Li et al. [6] observe that the prominence of viscoelastic behaviour is dependent on the film thickness.

Davies and Li [7] have shown that pressure thickening of the oil film is dominant at high eccentricities of the journal. This is the opposite of the temperature thinning that is dominant at low eccentricities. The thinning of the viscosity decreases and the thickening increases the eccentricity of the journal.

Inertia has also been shown to influence the dynamics of the bearing significantly. In the modelling of the large-scale journal bearings of heavy duty turbines, it has been shown that it is of significance to account for temperature mixing due to turbulence on the bearing [8].

The various dependencies and their influence on bearing dynamics have been highlighted extensively in literature. Accounting for dependencies has been shown to be crucial in accurately modelling the bearings. The influence of various dependencies acting in a system simultaneously and being allowed to interact with one another, has so far been neglected, however.

This paper considers the multi-physics problem, namely the influence of temperature and pressure when the velocity, temperature and stress fields are fully coupled. Coupled fields, in the context of this study, are fields which mutually influence the behaviour of one another. In this study, the allowed interaction was increased in order to determine the influence of these interactions on the flow characteristics. A full-scale simulation of the latter would have been computationally expensive. For this reason, we proceed with the following premise: consider a section of the bearing fluid film that exhibits the greatest dependencies. If coupling the governing equations has no significant influence, we can conclude that overall coupling would not influence the dynamics of the bearing. If, however, we find a significant change in the fluid behaviour, we can conclude that coupling would indeed influence the overall performance. The degree to which the bearing would be influenced, however, would have to be quantified by a full-scale simulation of the bearing.

The article is organised as follows: Section 2 presents the governing equations for four fluid models used to describe the oil film. Section 3 discusses the numerical implementation of the various models and Section 4 explains the numerical case to which these models are applied. The results obtained from the numerical study are presented in Section 5. Finally the results are compared and the influence of a coupled formulation is summarised in Section 6.

2. Governing Equations

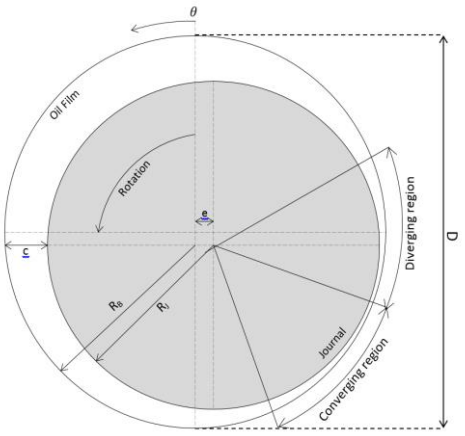

Figure 1: Schematic of a Journal bearing, front view.

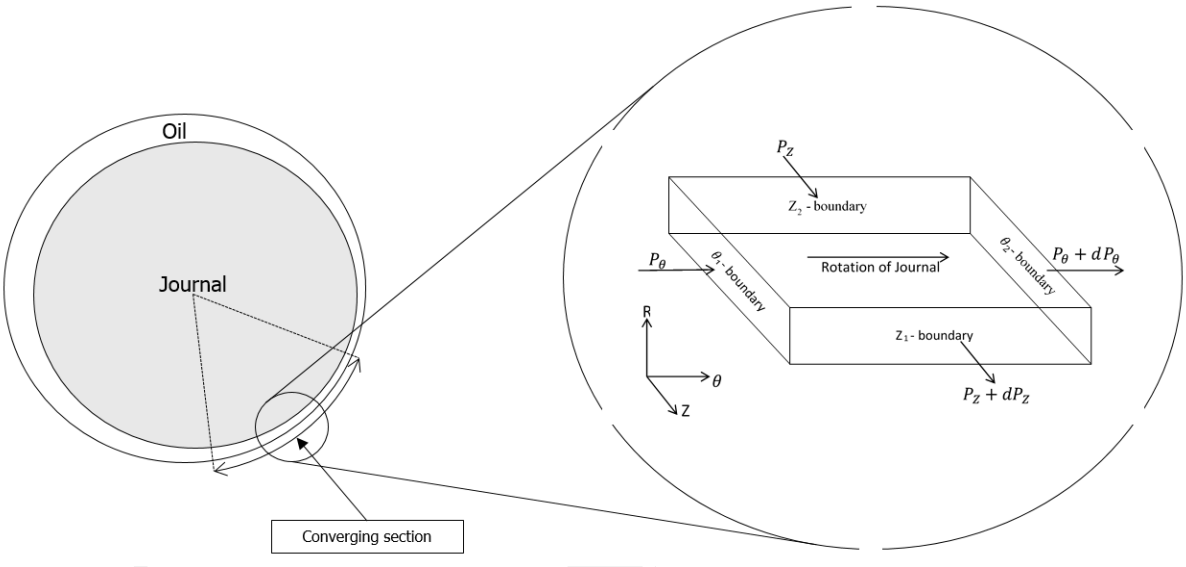

Figure 2: Schematic of bearing and the section of the film considered.

Consider Figure 1 which represents a bearing, where eccentricity is indicated as *e*, *c* refers to the film thickness, R_B and R_J refer to the bearing and journal radius respectively, and *D* is the diameter of the bearing. The section of the fluid film that is considered specifically in this article is extracted from the converging section of the bearing as illustrated in Figure 2.

This work used four distinct fluid models to describe the fluid dynamics of the oil film. All the fluid models considered were, however, assumed to be incompressible. The continuity equation therefore reduces to a condition of zero divergence in the velocity field:

$$\rho \nabla \cdot \bar{v} = 0 \tag{1}$$

The equation of motion used in this work is the Cauchy equation of motion with body forces neglected:

$$\rho \left(\frac{\partial v_i}{\partial t} + \sum_{j=1}^{3} v_j \frac{\partial v_i}{\partial x_j} \right) = \frac{\partial \sigma_{i,j}}{\partial x_j} \tag{2}$$

Here ρ is the density of the fluid, v_j is a component of the velocity vector, t is time, x_j is a component of the spatial vector and $\sigma_{i,j}$ is a component of the Cauchy stress tensor. The various formulations are determined primarily by the manner of dealing with the Cauchy stress tensor.
Since the models in this work are considered to be non-isothermal, the energy equation is also employed. This equation is coupled either strongly (through cross-terms appearing in each of the governing equations as well as the inconstancy of the fluid properties) or weakly (dependencies only influence the fluid properties which do not remain constant). The energy equation employed in this work has the form:

$$\rho C_p \left(\frac{\partial T}{\partial t} + \sum_{j=1}^{3} v_j \frac{\partial T}{\partial x_j} \right) = \frac{\partial}{\partial x_j} \left[k \frac{\partial T}{\partial x_j} \right] + Q \tag{3}$$

The last term, Q, represents heat generation inside the fluid film. Its form varies between the formulations.

2.1 Viscous fluid models

The first two formulations are viscous fluid formulations. The formulations assume a linear relationship between the rate-of-strain tensor and the velocity gradient tensor [9]. These formulations account for some of the dependencies arising from the polymer additives, but they neglect the elasticity of the polymers: therefore the fluid is purely viscous with no elasticity. The Cauchy stress tensor for the viscous formulation is:

$$\sigma_{ij} = -\delta_{i,j}\, p + \eta\, \dot{\gamma}_{i,j} \tag{4}$$

The Cauchy stress tensor and the rate-of-deformation tensor are related by a scalar, namely the viscosity denoted by η. The rate-of deformation, $\dot{\gamma}_{i,j}$, is of the form [10]:

$$\dot{\gamma}_{i,j} = \left(\frac{\partial v_i}{\partial x_j} + \frac{\partial v_j}{\partial x_i} \right) \tag{5}$$

The information about the material properties is contained in the viscosity. This model is a generalised Newtonian formulation of the fluid. This was the first model employed in this work.

The second model is a Stokes formulation with a generalised Newtonian constitutive relation. It is therefore similar to the previous model as far as the constitutive relation is concerned but the inertia terms are omitted from the equation of motion, Equation *(2)*. This construction is representative of the classical formulation, the Reynolds equation, applicable in the case of an uncoupled formulation[3]. This formulation is used as a comparison with the other formulations used in this study.

The heat generation term in *(3)* for the viscous formulation is of the form:

$$Q = \eta\, \dot{\gamma}_{i,j} \frac{\partial v_i}{\partial x_j} \tag{6}$$

The viscous fluid formulation is weak if the viscosity is a function of pressure, temperature and shear rate. If the viscosity is assumed to be constant, the fluid formulation is uncoupled.

2.2 Viscoelastic fluid models

Two viscoelastic fluid models were employed in this work. When modelling a viscoelastic fluid, the elastic component of the polymers is no longer neglected. The fluid is therefore modelled as having both viscous and elastic properties. This requires an additional governing equation to describe the

stress field of the polymer network [11]. This model considered the influence of the dependencies of the fluid properties and also the elastic properties of the polymer additives.

This work used differential constitutive relations to describe the polymer stress field. These equations were used because they are the simplest non-linear constitutive relations describing viscoelastic behaviour [12].

The extra stress tensor in the Cauchy stress tensor can be decomposed into the solvent and polymer contributions as follows [11]:

$$\sigma_{i,j} = -\delta_{i,j}\, p + \tau_{p(i,j)} + \tau_{s(i,j)} \tag{7}$$

The solvent contribution is similar to the generalised Newtonian formulation since it has the same linear relationship between the extra-stress tensor and the rate-of-deformation tensor. Though the linear relationship is also described by the viscosity, in the viscoelastic formulation a distinction is made between the solvent viscosity and the polymer viscosity.

The Giesekus constitutive model forms part of a large number of constitutive relations that extend the Oldroyd-B constitutive relation by adding an additional term. This additional term deals with the lack of shear thinning behaviour as well as a bounded extensional viscosity encountered with the Oldroyd-B model. The general form of these non-isothermal constitutive relations are [11], [13], [14]:

$$\tau_{p(i,j)} + f_{i,j}\left(\tau_{p(i,j)}, \dot{\gamma}_{i,j}\right) + \lambda(T)\frac{T_0}{T}\left[\frac{\delta\tau_{p(i,j)}}{\delta t} - \tau_{p(i,j)}\frac{Dln(T)}{Dt}\right] = \eta(T)\,\dot{\gamma}_{i,j} \tag{8}$$

The time derivative in (8) refers to the upper-convected derivative. This derivative makes the differential constitutive relation non-linear. It is necessary since it is independent of the superposed rotation of the polymer in the fluid. The upper-convected derivative has the form [15]:

$$\frac{\delta\tau_{p(i,j)}}{\delta t} = \frac{\partial\tau_{p(i,j)}}{\partial t} + v_k\frac{\partial\tau_{p(i,j)}}{\partial x_k} - \tau_{p(k,j)}\frac{\partial v_i}{\partial x_k} - \tau_{p(i,k)}\frac{\partial v_j}{\partial x_k} \tag{9}$$

Two viscoelastic formulations are used in this work: the Giesekus model and the Oldroyd-B formulation. The Giesekus model $f_{i,j}\left(\tau_{p(i,j)}, \dot{\gamma}_{i,j}\right)$ which is equal to $\alpha\frac{\lambda}{\eta_p}\tau^2_{p(i,j)}$ in (8) is set to zero.

The non-isothermal formulation of the constitutive relation presents a strongly coupled problem where the momentum equations (*2*), the energy equation (*3*), and the constitutive relation for the stress field (8) are all strongly coupled. This coupling can be made weaker by neglecting the temperature terms in (8) and by setting the fluid parameters as constants.

The heat generation term in (*3*) for the viscoelastic formulation is of the form:

$$Q = \tau_{s(i,j)}\frac{\partial v_i}{\partial x_j} + \phi\tau_{p(i,j)}\frac{\partial v_i}{\partial x_j} + (1-\phi)\frac{trace\left(\tau_{p(i,j)}\right)}{2\lambda(T)} \tag{10}$$

The equation of motion is strongly dependent on the differential constitutive relation. This relationship introduces a strong coupling between the momentum field and the polymer stress field. The viscoelastic formulation can be made weaker by neglecting the thermal terms in the constitutive relation and by holding the fluid properties constant.

2.3 Fluid properties

In order to describe the change in a fluid property caused by pressure and temperature, a shift factor, a_T, is defined with respect to some reference value of the fluid property in question. The fluid property as a function of temperature is described by the Williams-Landel-Ferry equation [16]:

$$a_T = \exp\left(-\frac{C_1(T - T_0)}{C_2 + T - T_0}\right) \tag{11}$$

T and T_0 refer to the temperature and the reference temperature respectively. The pressure dependence is described by the Barus law [1], [11]. These equations are combined into one shift factor; this is simply done as the form of both equations is that of an exponential function:

$$a_T = exp\left(-\frac{C_1(T - T_0)}{C_2 + T - T_0} - \frac{1}{3}\psi trace(\sigma)\right) \tag{12}$$

The reference values were chosen according to the data available. Here the value was chosen as T_0=300K and the reference pressure was the gauge pressure.

For the viscous model the shear thinning behaviour of the fluid is described by the Carreau model [16]. The shift factor is then applied to the Carreau model to describe the three-fold dependency of the viscosity.

$$\eta(\dot{\gamma}) = \frac{a_{T,P}\,\eta_0}{(1 + (a_T K_s\,\dot{\gamma})^b)^a} \tag{13}$$

In deriving the viscoelastic formulation, it is assumed that the solvent is a Newtonian fluid. The solvent and polymer viscosity are therefore a function only of pressure and temperature. The relaxation time will have a dependence on pressure and temperature similar to the dependence of the viscosity. These shift factors are applied as follows [17]:

$$\eta_t(T, p) = a_{T,P}\,\eta_t(T_0) \tag{14}$$

$$\lambda(T) = a_{T,p}\,\lambda\,(T_0) \tag{15}$$

3. Numerical Implementation

3.1 Viscous model implementation

The generalised Newtonian constitutive relation was rewritten in order to implement the viscous fluid formulation effectively in the OpenFOAM environment. The primary concern when casting the constitutive relation into a new form is the implicit evaluation of the terms. The divergence of the stress field in Equation *(2)* of the viscous constitutive relation, Equation (4) is:

$$\frac{\partial \sigma_{i,j}}{\partial x_j} = -\frac{\partial p}{\partial x_i} + \frac{\partial}{\partial x_j}\left(\eta\,\dot{\gamma}_{i,j}\right) \tag{16}$$

The divergence of the rate-of-deformation tensor can be simplified by using the fact that the divergence of the velocity field is zero for an incompressible fluid. This simplification leads to:

$$\frac{\partial}{\partial x_j}\left(\eta\,\dot{\gamma}_{i,j}\right) = \left(\frac{\partial \eta}{\partial x_j}\,\dot{\gamma}_{i,j}\right) + \eta\frac{\partial^2 v_j}{\partial x_j^2} \tag{17}$$

The second term on the right of Equation (17) is the Laplacian of the velocity field. This can be evaluated implicitly in the momentum equation in OpenFOAM. The rate of deformation can also be simplified by using the implication of incompressibility. The rate-of-deformation tensor is left as in Equation (17) in order to stabilise the numerical scheme [18].

The PISO (Pressure Implicit with Splitting Operator) was used in order to solve the governing set of equations for the viscous fluid formulation [19]. This algorithm executes as follows:

a) Compute the velocity field from the initial pressure field or from the pressure field computed in the previous time step.
b) Correct the pressure field by using the newly computed velocity field and applying the continuity condition to the equation.
c) The velocity field is corrected on the basis of the corrected pressure field.
d) Correct the mass flux at the boundaries according to the preservation of mass in the system.
e) Compute the temperature field from the energy equation using the new velocity field.
f) Adjust the viscosity according to the pressure, temperature and shear rate dependencies.
g) Repeat steps (a) to (f) until the momentum and the energy equation have converged below a specified residual.

The PISO algorithm is sufficient to deal with the viscous formulation for both the weak and the strong couplings.

3.2 Viscoelastic model implementation

The divergence of the extra stress tensor τ_p in the momentum equation *(2)* poses a difficulty with its evaluation in the time domain. If the divergence of this tensor is taken directly in OpenFOAM without further ado, it is evaluated explicitly since the only field that is evaluated implicitly in solving the momentum equation *(2)* would be the velocity field. The explicit evaluation of the extra stress tensor introduces instability to the system; so the DEVSS (Discrete Elastic Viscous Split Stress) decomposition is employed in order to stabilise the numerical solution. The momentum equation for the viscoelastic formulation is simply derived by substituting (17) into (7) and substituting the result in the equation of motion *(2)*. This yields:

$$\rho\left(\frac{\partial v_i}{\partial t}+\sum_{j=1}^{3} v_j\frac{\partial v_i}{\partial x_j}\right)-\eta_s\frac{\partial^2 v_j}{\partial x_j^2}=-\frac{\partial p}{\partial x_i}+\frac{\partial \tau_{p(i,j)}}{\partial x_j}+\dot{\gamma}_{i,j}\frac{\partial \eta_s}{\partial x_j} \tag{18}$$

The DEVSS decomposition is implemented by adding a Laplacian term on both sides of Equation (*18*). The Laplacian term is multiplied by the polymer viscosity so that the total viscosity (the sum of the solvent and polymer viscosities) appears in the momentum equation.

$$\rho\left(\frac{\partial v_i}{\partial t}+\sum_{j=1}^{3} v_j\frac{\partial v_i}{\partial x_j}\right)-\eta_t\frac{\partial^2 v_j}{\partial x_j^2}=-\frac{\partial p}{\partial x_i}+\frac{\partial \tau_{p(i,j)}}{\partial x_j}+\dot{\gamma}_{i,j}\frac{\partial \eta_s}{\partial x_j}-(1-\beta)\eta_t\frac{\partial^2 v_j}{\partial x_j^2} \tag{19}$$

β denotes the ratio between the solvent viscosity and the total viscosity (the total viscosity is the sum of the solvent and polymer viscosities).The Laplacian term on the left-hand side is evaluated implicitly whereas the new term on the right-hand since is evaluated explicitly. The Laplacian term on the left hand side is added to the diagonal components of the discretised matrix. This strengthens the diagonal dominance of this matrix and in this way improves the numerical stability.

Due to the additional coupled field introduced in the viscoelastic formulation form, the viscous formulation the PISO algorithm cannot be applied as was done in the previous section. The non-linear system has to be linearised in each time step by setting the coefficients as constants in the governing equations in each time step. This is done by using the inbuilt function ".relax()" in OpenFOAM. The governing equation is then solved and the coefficients are updated after the governing equations have been solved. The algorithm is executed as follows:

a) The shift factor is applied to the viscosity and the relaxation time.
b) The nonlinear momentum equation is updated and linearised (relaxed).
c) The linearised momentum equation is solved.
d) The pressure correction equation is solved and the pressure field is corrected accordingly.
e) The pressure equation is linearised (relaxed) in order to correct the momentum equation.
f) The differential constitutive relation is updated and linearised (relaxed).
g) The linearised constitutive relation is solved.
h) Compute the energy equation for the temperature field, using all the latest computed fields.
i) Steps (a) to (h) are repeated until a converged solution is obtained.

3.3 Validations

Since the formulation had been newly implemented in OpenFOAM, it had to be validated. To this end, known closed-form solutions were used. Firstly it was established that the uncoupled Stokes formulation was a good representative of the classical Reynolds equation when the film thickness is small: The error was found to be 0.682% if the clearance of the bearing was 1 mm. This comparison was made by using the long bearing approximation to solve the Reynolds equation. The computational domain solved by the Stokes formulation was therefore two-dimensional. The error was observed to decrease as the clearance of the bearing decreased. This is due to the assumption that the film thickness is negligible when deriving the Reynolds equation. Therefore, as the bearing clearance is decreased the aforementioned assumption is more closely approximated.

The solution of two concentric rotating cylinders was used in order to validate the accuracy of the velocity profile and the temperature profile. It was found that the highest errors were 0.261% and 0.122% for the velocity and temperature profiles respectively on a mesh for which mesh independence had been established.

The solution to a simple channel flow problem, where a pressure gradient is set over two parallel walls, was used to validate the shear thinning behaviour of the fluid. Errors of 0.118% and 0.0412% were obtained for the viscous formulation with and without inertia respectively.

The simple Couette flow setup was used to validate the stress field of the viscoelastic solvers. Two infinite parallel plates, one moving and one stationary, were modelled. It was found that in both formulations the error of the predicted stress field was less than 0.01% for all the tensor components.

3.4 Numerical case

Large-scale journal bearings pose a particular challenge in terms of the computational resources required. The reason is that the film is very thin compared to the other dimensions of the bearing, and the circumference and the length of the bearing are up to three orders of magnitude larger than the film thickness. Achieving a stable converged solution would require an excessively large number of Control Volumes (CVs). Since the number of CVs are much higher than what are practically possible another approach had to be taken.

Instead of considering the entire film, only a section of the film was considered. This was done with the particular purpose of establishing the extent of the influence of a coupled formulation. Extrapolating the global influence of a coupled formulation based on such a section would be quite unreasonable without considering this matter in itself. However, if a section of the film is considered where the fluid dependencies are expected to be the highest and it is found that a coupled formulation in this section is negligible, then this would indicate that a coupled formulation would not significantly influence the bearing operating condition. By contrast, it is noted that the largest contribution of the bearing's capacity to bear load is determined by the pressure in the converging section of the bearing. As the eccentricity of the journal bearing increases, the maximum pressure moves in the direction of the diverging section. The long bearing solution shows that the load-carrying capacity of the bearing is determined by a decreasing section of the converging area as the eccentricity increases. Changes in this region of the bearing therefore have important implications for the bearing's operating conditions, even though it is difficult to quantify the extent of the influence by considering only such a small section of the film.

In order to have a proper representation of the particular region of the film, the factors that influence the fluid dynamics in the extracted region must be a reasonable approximation of the actual flow condition in the bearing. Figure 3 shows the extracted region of the film with the important factors that influence the flow indicated on the figure. These factors are determined by looking at the Reynolds equation:

$$\frac{\partial}{\partial\theta}\left[b_1(\theta)\,\frac{\partial p}{\partial\theta}\right]+\frac{\partial}{\partial Z}\left[b_2(\theta)\frac{\partial p}{\partial Z}\right]=b_3(\theta) \tag{20}$$

where the coefficients of the Reynolds equation are:

$$b_1(\theta)=(1+\epsilon\cos\theta)^3 \tag{21}$$

$$b_2(\theta)=\left(\frac{R}{2L}\right)^2(1+\epsilon\cos\theta)^3 \tag{22}$$

$$b_3(\theta)=-\frac{6\eta\omega R^2\epsilon}{c^2}\sin\theta \tag{23}$$

The bearings considered operate at 3000 rpm because the power line frequency is 50 Hz. The top wall of the computational domain, presented in Figure 3, should therefore move at an equivalent velocity, which translates into a velocity of 80 m/s (see Table 3 for bearing specifications).

The bearings that were considered in this study are for large turbo generators. Fluctuations in the operating conditions in these kinds of machines would result in a fluctuation in electricity generation as well as in line frequency. Therefore great care is taken in order to ensure the proper control of the rotational speed of the turbine.

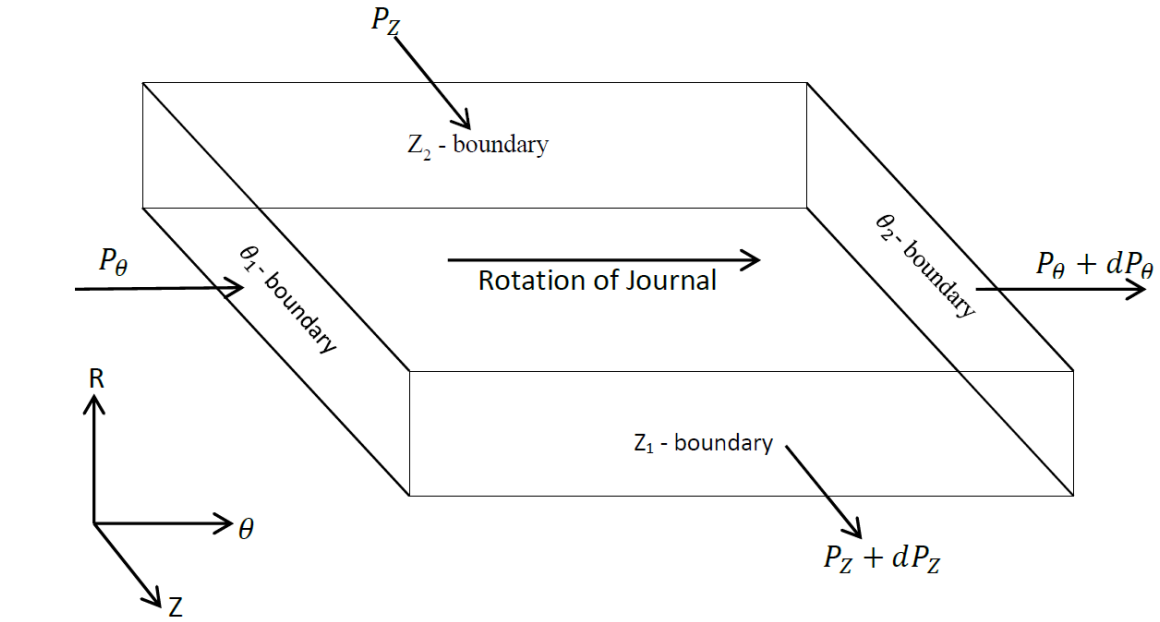

Figure 3: Representation of computational domain with primary factor influencing flow indicated.

Determining the pressure boundary conditions is not as simple as determining the boundary condition of the moving wall. The pressure at each of the walls has to be determined in order to find reasonable pressure boundary conditions. This was done by using the Finite Difference Method (FDM) to solve the Reynolds equation (20). The nodes in the mesh used with the finite difference method were set so that the nodes were located at each of the boundaries. This is illustrated in Figure 3.

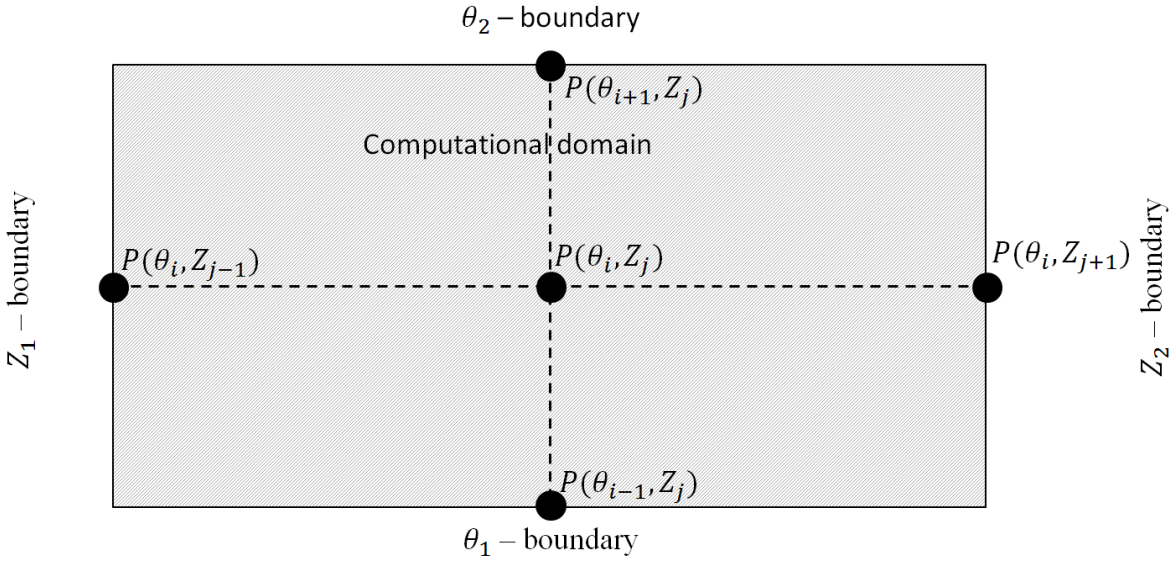

Figure 4: Computational domain, indicating the pressure nodes from the FD mesh.

The pressure computed was taken to be the constant pressure over the wall, with the θ_2-boundary set at zero gradient boundary condition. This caused the θ_2-boundary to yield a linear gradient from the high-pressure wall to the low-pressure wall. This avoided having two corners in the computational domain where the high and low pressures meet. The nodes selected were at the centre of the bearing and therefore corresponded to the region of the maximum pressure in the bearing. The pressures at each of the nodes are presented in Table 1.

Table 1: Pressure boundaries and corresponding values, computed using the FDM.

Boundary	Computed pressure [m^2/s^2]
$p(\theta_1)$	2.5350×10^4
$p(\theta_2)$	2.5354×10^4
$p(Z_1)$	2.5355×10^4
$p(Z_2)$	2.5334×10^4

The pressure values used in this study were located at the centre of the bearing. This implies that the axial pressure gradient over the computational domain was lower than at the edges of the bearing. In the case of high eccentricities it was seen that the pressure dropped rapidly as the oil moved from the converging section of the bearing to the diverging section.

The specifications of the bearing that was considered are given in Table 2.

Table 2: Bearing specifications.

	Value
Average bearing clearance (c)	1mm
Journal diameter ($2R_J$)	998mm
Bearing diameter ($2R_B$)	1000mm
Eccentricity ratio (ϵ)	0.8
Angular velocity of journal (Ω)	3000rpm

The dimensions of the computational domain and the fluid properties that were used are listed in Table 3.

Table 3: Computational domain and fluid property specifications.

Film thickens (height of domain)	0.4 mm
Length and width of computational domain	2 mm
First WLF constant (C_1)	-5.898
Second WLF constant (C_2)	-266.967
Reference temperature(T_0)	300K
Pressure dependence constant (ψ)	1.4924 x 10^{-5} s^2/m^2
First Carreau constant (a)	0.3
Second Carreau constant (b)	0.25
Mobility constant for Giesekus model (α)	0.5
Solvent polymer viscosity ratio (β)	0.77
Relaxation time (λ)	0.012s
Zero shear viscosity of oil (η_0)	10.48 x 10^{-3} mm^2/s

The velocity boundary conditions at the top and bottom plate were no-slip boundary conditions. Zero gradient boundary conditions were selected for the velocity at each of the Z_i and θ_i boundaries.

The thermal boundary conditions for the non-isothermal case presented in Section 4.2 were selected to be at a constant temperature. The top and bottom plate were at 300 K and 350 K respectively, with zero gradient boundary conditions at the Z_i and θ_i boundaries. The shaft of the turbine would

be close to ambient temperature near the bearing [3]. For this reason, the top plate was set at slightly higher than ambient temperature. The temperature at the bottom plate corresponded to the maximum temperature expected in the bearing. The oil that flows through this section will be close to this temperature [4]. Since the system is at steady-state conditions, the bearing wall would be very close to this temperature.

4. Results and discussion

Two specific couplings were considered for the four fluid models respectively. The first coupling was pressure and shear rate dependencies. This is a weak coupling where the coupling of the equations is primarily due to fluid properties which change according to the aforementioned dependencies.

A strong coupling was considered when the system was deemed to be non-isothermal. The coupling is introduced into the equations not only through the fluid properties but also through the cross-terms appearing in the governing equations. In such a case, one governing equation is directly influenced by another and vice versa. Also in such a case, information is constantly exchanged between the governing equations.

The velocity profile was computed for each of the formulation at the centre of the computational domain. The domain dimensions were selected so that entry effects would not influence the velocity profiles measured at the centre of the domain. The magnitude of the velocity was taken. The velocity of the lubricant in the axial direction was seen to be at least two orders of magnitude smaller than in the circumferential direction. The reason was that the axial pressure gradient along the centre line of the bearing would be a minimum. This gradient would increase when moving closer to the ends of the bearing. The velocity, in the axial direction, close to the ends of the bearing would therefore be expected to be much higher than it had been computed to be along the centre line of the bearing. The differences between the various models were determined by comparing the results to those of the classical model.

A mesh convergence study was conducted for each of the cases presented in the following sections. Mesh independence was established for each case. The time steps and mesh specifications used in this study are presented in Table 4.

Table 4: Specifications for numerical simulations.

Time step size for weakly coupled formulation	1×10^{-5} s
Time step size for strongly coupled formulation	1×10^{-7} s
Number of CVs in mesh	50 000

4.1 Pressure dependence

In this section, the fluid models are considered in the light of the pressure and shear rate dependence of the fluid. The analysis in this section is therefore isothermal. The pressure and shear rate dependencies of the viscosity introduce an additional non-linearity to the fluid problem. Describing a coupling as strong or weak is a rather subjective matter[20]. In the current study, the pressure and shear rate dependencies were considered as introducing a weak coupling: the viscosity is determined by the field variables computed from the governing equations. The governing equation was then updated according to the newly calculated viscosity from its constitutive relation. The viscosity relation does not add another governing equation; rather it is added in order to complete the set of governing equations.

The velocity profiles computed were obtained by plotting the magnitude of the velocity in the radial direction. The radial position is put in non-dimensional form by dividing the radial position by the bearing clearance. The classical model is computed by using an uncoupled model and using the reference values of the fluid properties. An uncoupled model is also presented in Figure 5: this is similar to the classical model. The fluid properties used in the computation were determined by taking the average value of the fluid properties when pressure and shear rate were taken into account. The fluid properties were then held constant at these determined values. This was a way to determine the influence of the coupling.

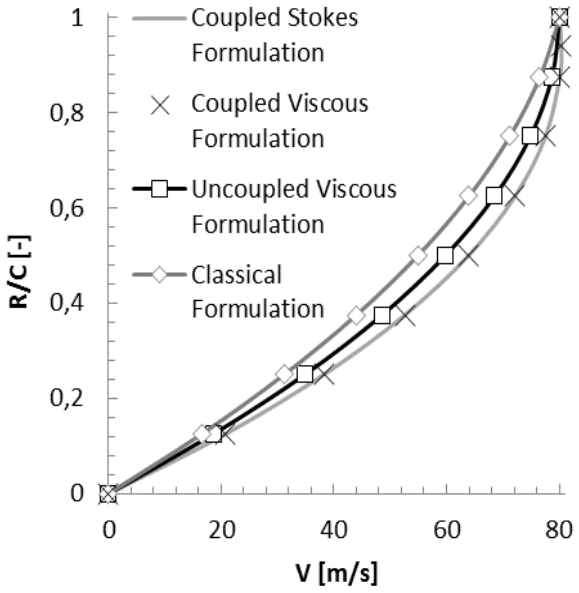

Figure 5: Velocity profiles from the viscous fluid model.

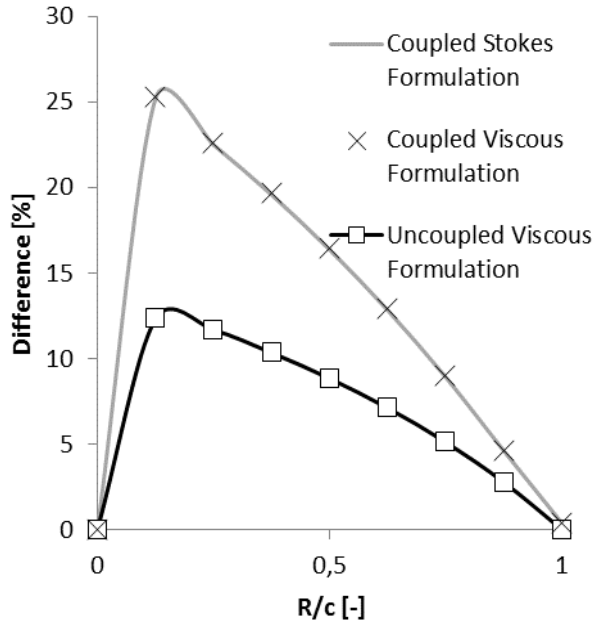

Figure 6: Comparison of the viscous fluid and classical model.

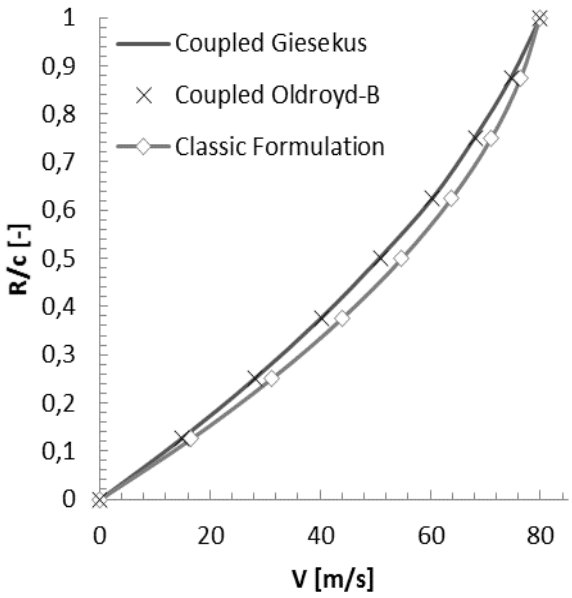

Figure 7: Velocity profiles for the viscoelastic and classical models.

The difference between the coupled and the classical and uncoupled formulations can be determined using the classical formulation as a reference. The results were computed as a percentage difference between the classical model and the viscous and viscoelastic models.

The results obtained from this analysis were plotted against the non-dimensionalised radial position and are presented in Figure 6 for the weakly coupled viscous models.

Figure 6 shows a uniform change in flow when the models depart from the classical model. This is even the case with the coupled models. Through the difference between the coupled models was found to be negligible, a significant difference was seen between the coupled and uncoupled models. The coupling produced double the difference when compared to the uncoupled model.

Similarly the velocity profiles for the weakly coupled viscoelastic models are shown in Figure 7.

The viscoelastic models are compared to the classical model in the same way as was done with the viscous model. The difference functions of the viscoelastic model are presented in Figure 8.

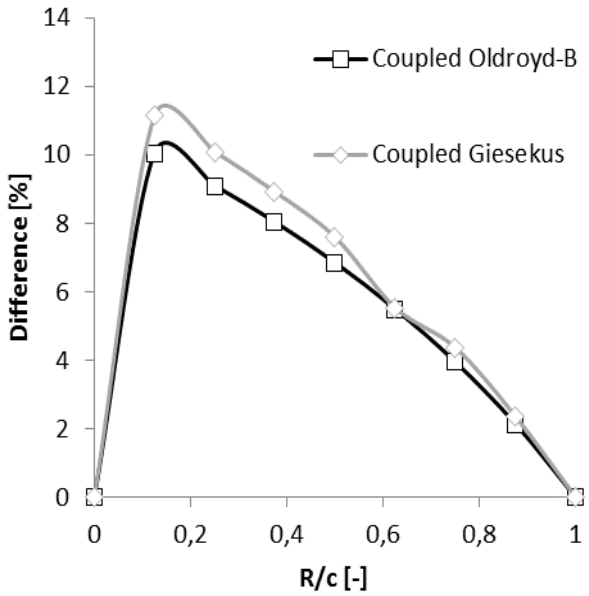

Figure 8: Comparison of the viscoelastic fluid and classical models.

Although both of the viscoelastic models are coupled, this coupling cannot be weakened or strengthened because the constitutive relation is coupled with the momentum equation. For this reason, comparing the coupling between the viscoelastic models is more a question of comparing a weak coupling to a weaker coupling, instead of comparing a coupled model to an uncoupled model. The coupling in the Oldroyd-B case is weakened by setting the fluid properties to be constant. The values of these fluid properties were determined by finding the average value of the properties when pressure dependence was considered. It can be seen that, in the case of the stronger coupling (the Giesekus model), the departure from the classical formulation is no longer uniform. This implies that the character of the flow is changing. When this kind of non-uniform change in the flow occurs, care must be taken when taking the coupling into account. In the current case, the difference is quite small, but this might not be the case in general. Consequently a mere adjustment to the computed values may not be adequate to account for the coupling.

The difference between the viscoelastic fluid models is of the same order as in the uncoupled case in the viscous model, when compared to the classical model. The coupling of the viscous models is seen to have the greatest difference when compared to the classical model. It is only in the viscoelastic case, however, where a non-uniform change in the flow is observed.

4.2 Temperature dependence

This section considers non-isothermal fluid models. The fluid models are consequently considered as being strongly coupled. The strong coupling is introduced by the additional governing equations, and by the cross-terms appearing in the different governing equations. For the viscous model, the coupling is two-fold where both the momentum and energy equations are strongly coupled. In the viscoelastic case, the coupling is three-fold where the momentum, energy and constitutive equations are all coupled with one another.

The velocity profile was determined and the comparison made with the classical formulation in a fashion similar to the method used in the previous section.

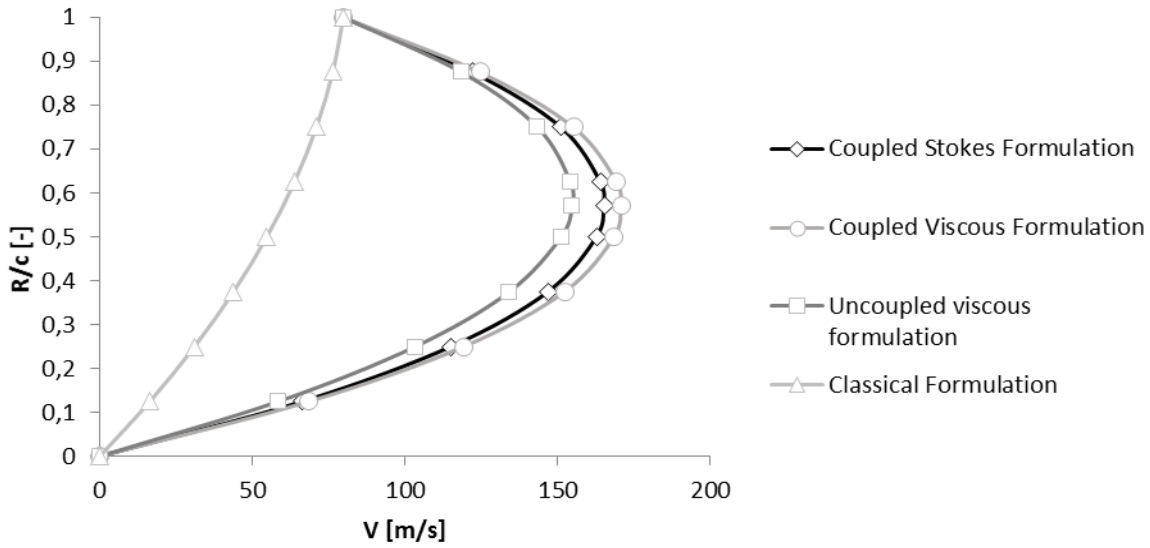

Figure 9: Velocity profiles computed from the viscous and the classical models.

It is clear from Figure 9 that there is a dramatic difference between the classical formulation and the viscous formulation.

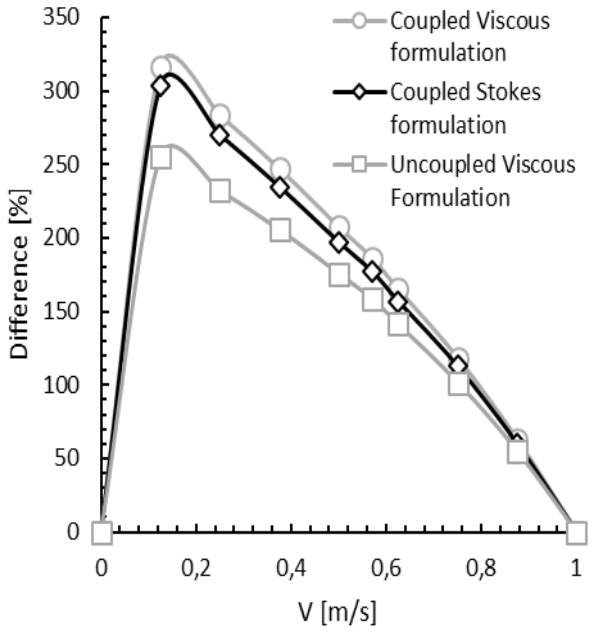

Figure 10: Comparison between the classic and viscous fluid models.

When the strong coupling is compared to the classical model, as is the case in Figure 10, it can be seen that there is a large increase in the percentage difference in comparison to the percentage differences obtained with the weak couplings (see Figure 6). Therefore a major departure from the classical model is caused by taking into consideration the temperature dependence. It is seen that there is a difference of about 20% between the coupled and uncoupled models. It is also seen that there is a departure from the homogeneous change from the classical model observed in the weakly coupled case. The strong coupling therefore introduces more than merely a mere change in the velocity of the field; the change in the velocity is not uniform and therefore the presence of the strong coupling changes the character of the flow.

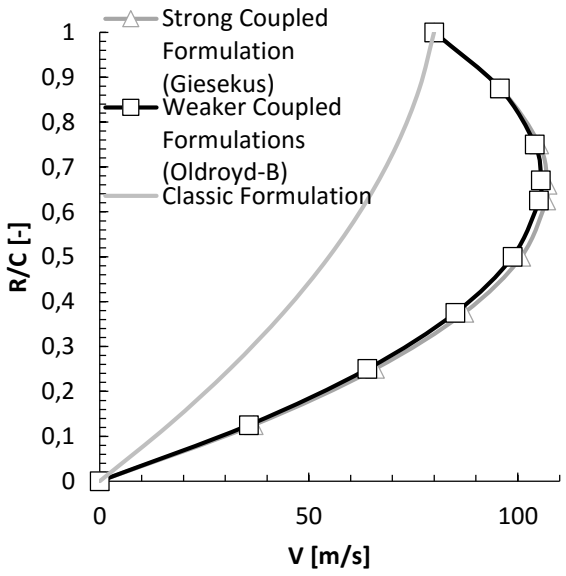

Figure 11: Velocity profiles for the viscoelastic models.

The viscoelastic models also show a strong departure from the classical model in comparison

Figure 12: Comparison between the classical and the viscoelastic fluid models.

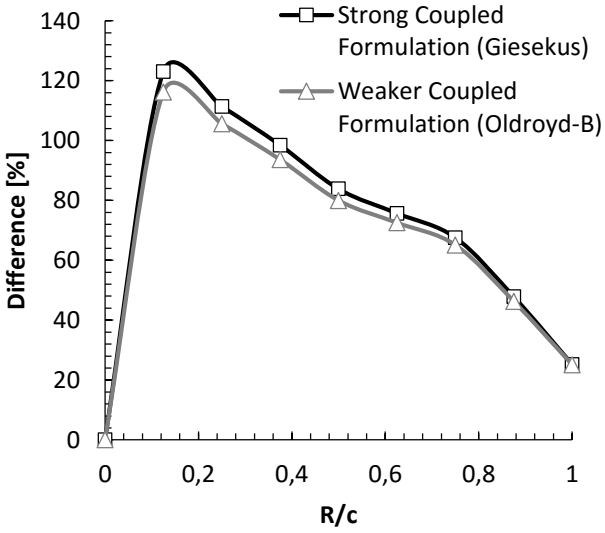

to the weaker coupling presented in Section 4.1 as seen in Figures 11 and 12.

The greatest departure from the character of the classical model is shown in Figure 12 with the strongly coupled viscoelastic fluid model. Both of the viscoelastic models showed a significant departure from the character of the flow of the classical model. Though the difference is not as great as with the viscous model the departure from the classical model with the viscous model is more uniform than in the case of the viscoelastic model.

The influence of the coupling is not the same in Section 4.1 and 4.2. Although the coupling is stronger the dependencies are also seen to exert a different influence on the flow. This implies that the dependency will also affect the influence and extent of the coupling. The weak coupling in the viscous model affects the flow more than is the case with the strong coupling. The weak coupling does not change the nature of the flow as was observed in the case of the strong coupling.

5. Conclusion

This work highlights the need to consider the coupling of equations when modelling large-scale journal bearings. The influence of the coupling was shown to depend on the fluid model, the dependency that introduces the coupling and the strength of the coupling.

The weak coupling changed the velocity of the flow quite significantly in the case of the viscous model. The character of the flow was seen to change for the viscoelastic model, although the change in the flow velocity was not as dramatic.

The temperature dependence showed the greatest change in the velocity of the flow in comparison to the classical model. Due to the strong coupling it was also seen to induce a departure from the character of the flow predicted by the classical model.

The influence of the coupling on the fluid behaviour differed in both the cases considered in this study. This shows that the coupling of equations cannot be treated in a generic way. Since the influence of the coupling is determined by the dependency that introduces the coupling, it follows that compensating for couplings in operating condition calculations is not a trivial matter: a mere adjustment of the computed values will not be sufficient. Although an adjustment might be trivial, sufficient care must be taken when applying such adjustments since these adjustments may not hold true in general. This is particularly clear in the case of the strong couplings, where the departure from the classical models was non-uniform.

More research is needed to quantify the influence of the coupling in a full-scale journal bearing, however, the evidence provided in this work shows emphatically that the coupling should be considred: since the region of the bearing considered has the greatest dependence of the fluid properties, the fact that the coupling influences the flow significantly shows that this line of research would require deeper analysis. Another important factor to consider regarding this region is that this region mainly influences the operating conditions of the bearing. This is especially true when the eccentricity of the bearing is high.

Acknowledgements

This work was financially supported by the Department of Mechanical and Aeronautical Engineering at the University of Pretoria.

References

[1] X. . Li, D. R. Gwynllyw, A.R. Davies, and T. Phillips, On the influence of lubricant properties on the dynamics of two-dimensional journal bearings, *J. Nonnewton. Fluid Mech.,* 93, no. 1, pp. 29–59, Sep. 2000.

[2] D. R. Gwynllyw and T. N. Phillips, The influence of Oldroyd-B and PTT lubricants on moving journal bearing systems, *J. Nonnewton. Fluid Mech.*, vol. 150, no. 2–3, pp. 196–210, Apr. 2008.

[3] A. Z. Szeri, *Fluid film lubrication,* vol. 2. Cambridge University Press Cambridge, 2011.

[4] X. . Li, A.R. Davies, and T. Phillips, A transient thermal analysis for dynamically loaded bearings, *Comput. Fluids*, vol. 29, no. 7, pp. 749–790, Jul. 2000.

[5] T. Mang, W. Dresel, *Lubricants and lubrication*. John Wiley & Sons, 2007.

[6] X. K. Li, Y. Luo, Y. Qi, R. Zhang, On non-Newtonian lubrication with the upper convected Maxwell model, *Appl. Math. Model.*, vol. 35, no. 5, pp. 2309–2323, May 2011.

[7] A. R. Davies, X. K. Li, Numerical modelling of pressure and temperature effects in viscoelastic flow between eccentrically rotating cylinders, *J. Nonnewton. Fluid Mech.*, vol. 54, no. 94, pp. 331–350, Aug. 1994.

[8] S. Uhkoetter, S. aus der Wiesche, M. Kursch, C. Beck, Development and validation of a three-dimensional multiphase flow CFD analysis for journal bearings in steam and heavy duty gas turbines, ASME Turbo Expo 2012: Turbine Technical Conference and Exposition, 2012, pp. 749–758.

[9] F. M. White, *Viscous fluid flow*, vol. 3. McGraw-Hill New York, 2006.

[10] J. N. Reddy, *Principles of continuum mechanics*, Cambridge University Press, 2009.

[11] R. G. Owens and T. N. Phillips, *Computational rheology*, vol. 2, no. 2. World Scientific, 2002.

[12] R. B. Bird, R. C. Armstrong, O. Hassager, Dynamics of polymeric liquids, 1977.

[13] E. Zhmayev, H. Zhou, Y. L. Joo, Modeling of non-isothermal polymer jets in melt electrospinning, *J. Nonnewton. Fluid Mech.*, vol. 153, no. 2, pp. 95–108, 2008.

[14] D. Thomas, R. Sureshkumar, B. Khomami, Effect of inertia on thermoelastic flow instability, *J. Nonnewton. Fluid Mech.*, vol. 120, no. 1–3, pp. 93–100, Jul. 2004.

[15] R. M. Christensen, *Theory of Viscoelasticity*, Courier Dover Publications, 2013.

[16] A. Wachs, J.R. Clermont, A. Khalifeh, Computations of non-isothermal viscous and viscoelastic flows in abrupt contractions using a finite volume method, *Eng. Comput.*, vol. 19, no. 8, pp. 874–901, 2002.

[17] F. Habla, H. Marschall, O. Hinrichsen, Numerical simulation of viscoelastic two-phase flows using openFOAM®, *Chem. Eng. Sci.*, vol. 66, no. 22, pp. 5487–5496, 2011.

[18] P. J. Oliveira, F. T. Pinho, and G. a. Pinto, Numerical simulation of non-linear elastic flows with a general collocated finite-volume method, *J. Nonnewton. Fluid Mech.*, vol. 79, no. 1, pp. 1–43, Sep. 1998.

[19] J. H. Ferziger, M. Peric, A. Leonard, Computational Methods for Fluid Dynamics, *Phys. Today*, vol. 50, no. 3, pp. 80–84, 2008.

[20] B. Markert, *Weak or strong: On coupled problems in continuum mechanics*, DIP - Digital Print, 2010.